

Bias-free model fitting of correlated data in interferometry

Régis Lachaume^{1,2*}

¹*Instituto de Astronomía, Facultad de Física, Pontificia Universidad Católica de Chile, casilla 306, Santiago 22, Chile*

²*Max-Planck-Institut für Astronomie, Königstuhl 17, D-69117 Heidelberg, Germany*

28 January 2021

ABSTRACT

In optical and infrared long-baseline interferometry, data often display significant correlated errors because of uncertain multiplicative factors such as the instrumental transfer function or the pixel-to-visibility matrix. In the context of model fitting, this situation often leads to a significant bias, which in the gravest cases can show a fit passing outside of all error bars. It is known in nuclear physics as Peelle’s Pertinent Puzzle. I show how this arises in the context of interferometry and how severe it can be in a realistic setting. I then give a conceptually simple and computationally cheap way to avoid the issue: model the data without covariances, estimate the covariance matrix by error propagation using the modelled data instead of the actual data, and, finally, perform the model fitting using the covariance matrix.

Key words: techniques: interferometric — methods: statistical

1 INTRODUCTION

Optical and infrared long-baseline interferometry consists in measuring the fringe contrast and phase of interference fringes in the recombined light collected at several telescopes¹. These observables hold information on the celestial object’s spatial properties, which are usually obtained through model fitting.

In spite of strong evidence of correlations in data, due to redundancy (Monnier 2007, in the case of closure phases), calibration (Perrin 2003), or atmospheric biases acting on all spectral channels in the same way (Lawson 2000), only a few authors (Perrin et al. 2004; Absil et al. 2006; Berger et al. 2006; Lachaume et al. 2019; Kammerer et al. 2020) have analysed correlated data while most assume independent errors. In particular, the only interferometric instrument I know of with a data processing software taking into account one source of correlations—calibration—is FLUOR² (at IOTA³, then CHARA⁴, Perrin et al. 2004). None of the five first and second-generation ones at the VLTI⁵ does (Millour et al. 2008; Hummel & Percheron 2006; Le Bouquin et al. 2011; ESO GRAVITY pipeline team 2020; ESO MATISSE pipeline team 2020). The same lack of support for correlations is present in image reconstruction programmes (e.g. MIRA, see Thiébaud 2008), model-fitting tools (e.g. Litpro, see Tallon-Bosc et al. 2008), or the still widespread first

version of the Optical Interferometric FITS format (OIFITS v. 1, Pauls et al. 2005).

Unfortunately, it has been shown that ignoring uncertainties may lead to significant errors in model parameters as Lachaume et al. (2019) evidenced with stellar diameters using PIONIER⁶ (Le Bouquin et al. 2011) data at the VLTI. Also Kammerer et al. (2020) established that correlations were necessary to achieve a higher contrast ratio in companion detection using GRAVITY (Eisenhauer et al. 2011) at the VLTI.

Several sources of correlated uncertainties occur in a multiplicative context, when several data points are normalised with the transfer function (Perrin 2003) or the coherent fluxes are derived with the pixel-to-visibility matrix formalism (Tatulli et al. 2007). In both cases, the uncertainty on the multiplicative factor translates into a systematic, correlated one in the final data product. In the context of experimental nuclear physics, Peelle (1987) noted that this scenario could lead to an estimate falling below the individual data points, a paradox known as Peelle’s Pertinent Puzzle (PPP). It results from the usual and straightforward, but actually incorrect, way to propagate covariances (D’Agostini 1994; Neudecker et al. 2012). A few workarounds have been proposed (e.g. Burr et al. 2011; Becker et al. 2012; Nisius 2014) but they are not straightforward.

The issue, however, not widely known in many other fields where the problem has seldom arisen. In this paper, I present the paradox within the context of long-baseline interferometry (Sect. 2), derive the order of magnitude of its effect using the modelling of a single value (Sect. 3), analyse in detail its

* regis.lachaume@gmail.com

¹ Recombination may be performed by software in the case of intensity interferometry or heterodyne detection.

² Fiber Linked Unit for Optical Recombination

³ Infrared and Optical Telescope Array

⁴ Center for High Angular Resolution Array

⁵ Very Large Telescope Interferometer

⁶ Precision Integrated-Optics Near-infrared Imaging Experiment

effect in least squares model-fitting (Sect. 4) and propose a simple, computer-efficient way to avoid it (Sect. 5).

2 PELLE'S PERTINENT PUZZLE BASICS

I rewrite and adapt Peelle's original example in the context of long-baseline interferometry. Let's assume the inverse of the instrumental fringe contrast $\tau \pm \tau\sigma_\tau$ has been interpolated from one or several calibrator observations. A visibility amplitude is now now estimated from two contrast measurements $\nu_1 \pm \sigma_\nu$ and $\nu_2 \pm \sigma_\nu$. For each measurement, visibility amplitudes are:

$$V_1 = \tau\nu_1 \pm \tau\sigma_\nu (\pm\tau\nu_1\sigma_\tau), \quad (1a)$$

$$V_2 = \tau\nu_2 \pm \tau\sigma_\nu (\pm\tau\nu_2\sigma_\tau). \quad (1b)$$

They are normalised with the same quantity (τ), so they are correlated, hence the systematic uncertainty term between parentheses in Eq. (1). Error propagation gives the covariance matrix

$$\Sigma = \begin{pmatrix} \sigma_\nu^2\tau^2 + \sigma_\tau^2\nu_1^2 & \sigma_\tau^2\nu_1\nu_2 \\ \sigma_\tau^2\nu_1\nu_2 & \sigma_\nu^2\tau^2 + \sigma_\tau^2\nu_2^2 \end{pmatrix}, \quad (2)$$

when the second-order error term ($\sigma_\nu\sigma_\tau$) is ignored. Using the matrix inverse Σ^{-1} , the least squares estimate is

$$V = \frac{(\Sigma_{11}^{-1} + \Sigma_{12}^{-1})V_1 + (\Sigma_{22}^{-1} + \Sigma_{12}^{-1})V_2}{(\Sigma_{11}^{-1} + \Sigma_{12}^{-1}) + (\Sigma_{22}^{-1} + \Sigma_{12}^{-1})}, \quad (3)$$

$$= \frac{V_1 + V_2}{2} \left(1 + \sigma_\tau^2 \frac{(V_1 - V_2)^2}{2\tau^2\sigma_\nu^2} \right)^{-1}.$$

It systematically falls below the average of the two values ν_1 and ν_2 . If measurements differ significantly, it can even fall below the lowest value. Figure 1 gives such an example with a instrumental visibility of 50% and two measurements on an unresolved target:

$$\begin{aligned} \tau &= 2.000 \pm 0.100 \text{ (5\%)}, \\ \nu_1 &= 0.495 \pm 0.003 (\approx 0.6\%), \\ \nu_2 &= 0.505 \pm 0.003 (\approx 0.6\%), \end{aligned}$$

which yields two points 2.4 standard deviations apart

$$\begin{aligned} V_1 &= 0.990 \pm 0.006 (\pm 0.050), \\ V_2 &= 1.010 \pm 0.006 (\pm 0.050) \end{aligned}$$

and the estimate

$$V = 0.986 \pm 0.004 (\pm 0.049)$$

falls outside the data range.

3 SINGLE VALUE FIT

Let's consider a set of measurements of a single normalised quantity, like the visibility amplitude, given by a column vector $\mathbf{v} = (v_1, \dots, v_n)^T$. It is derived from an uncalibrated quantity like the fringe contrast, $\boldsymbol{\nu} = (\nu_1, \dots, \nu_n)^T$

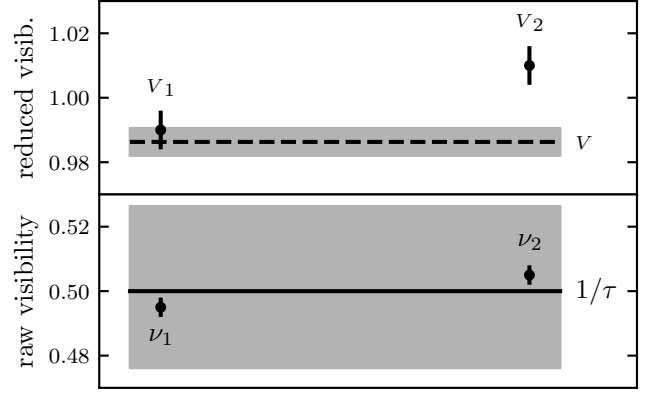


Figure 1. Original Peelle problem rewritten in the context of interferometry. *Bottom:* Two raw visibility amplitudes ν_1 and ν_2 (points with statistic error bars of $\approx 0.6\%$) are calibrated by the transfer function $1/\tau$ (solid line with systematic error zone of 5%). *Top:* the two calibrated visibility measurements V_1 and V_2 (points with statistic error bars of $\approx 0.6\%$) are strongly correlated. The least-squares estimate for the visibility V (dashed line, with statistic uncertainty error zone displayed) falls outside of the data range.

Table 1. Symbols used in this paper. Lower case bold font is used for vectors and upper case bold font for matrices.

Symbol	Meaning
\bar{a}	true value of a
$\langle a \rangle$	expectancy of a
\mathbf{A}^T	transpose of \mathbf{A}
$\mathbf{c} = \mathbf{a} \odot \mathbf{b}$	element-wise product of \mathbf{a} and \mathbf{b}
$\mathbf{C} = \mathbf{a} \otimes \mathbf{b}$	outer product of \mathbf{a} and \mathbf{b}
$\mathbf{c} = \mathbf{A}\mathbf{b}$	matrix product of \mathbf{A} and \mathbf{b}
δ	Kronecker delta
\mathbf{v}	data
$\boldsymbol{\eta}$	error ($= \mathbf{v} - \bar{\mathbf{v}}$)
σ^2	variance ($= \langle \eta^2 \rangle$)
Σ	covariance matrix ($= \langle \boldsymbol{\eta} \otimes \boldsymbol{\eta} \rangle$)
ϱ	correlation coefficient
\mathbf{x}, \mathbf{X}	sensitivity vector or matrix
\mathbf{p}	parameters of the model
$\boldsymbol{\mu}$	model values ($= \mathbf{X}\mathbf{p} \approx \bar{\mathbf{v}}$)
a_ν	a of the measurement error
a_τ	a of the normalisation error
a^*	a impacted by PPP

and a normalisation factor, like the cotransfer function, $\boldsymbol{\tau} = (\tau_1, \dots, \tau_n)^T$ by

$$\mathbf{v} = \boldsymbol{\tau} \odot \boldsymbol{\nu}, \quad (4)$$

where \odot denotes the Hadamard (element-wise) product of vectors. If $\bar{\mathbf{v}}$, $\bar{\tau}$, and $\bar{\nu}$ the true, but unknown, values of these quantities, the error vector on \mathbf{v}

$$\boldsymbol{\eta} = \mathbf{v} - \bar{\mathbf{v}}, \quad (5)$$

can be written as a sum of measurement and normalisation errors if one ignores a second-order term:

$$\boldsymbol{\eta} = \boldsymbol{\eta}_\nu + \bar{\mathbf{v}}\boldsymbol{\eta}_\tau. \quad (6)$$

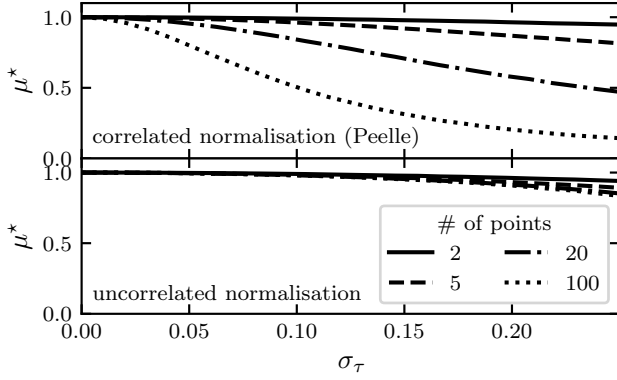


Figure 2. Fit μ^* to unresolved visibilities ($v = 1$), as a function of the relative uncertainty on the calibration σ_τ and the number of measurements n . $2/n \times 10^5$ simulations were made and averaged, assuming that η_ν and η_τ follow normal distributions. *Top*: fully correlated normalisation like in original Peelle’s puzzle ($\sigma_\nu = 0.02$ and $\varrho = 1$). *Bottom*: normalisation error without correlation ($\sigma_\nu = 0.02$ and $\varrho = 0$).

These errors are given by

$$\eta_\nu = \bar{\nu}(\nu - \bar{\nu}), \quad (7)$$

$$\eta_\tau = \frac{1}{\bar{\tau}}(\tau - \bar{\tau}). \quad (8)$$

Let’s assume η_ν and η_τ are independent error terms of mean 0 and standard deviations are σ_ν and σ_τ , respectively. In addition, I consider correlation of the normalisation errors, with correlation coefficient ϱ . In the case of interferometry, it can arise from the uncertainty on the calibrators’ geometry. The covariance matrix is given by

$$\Sigma = \langle \eta \otimes \eta \rangle, \quad (9)$$

where \otimes denotes the outer product of vectors and $\langle \rangle$ stands for the expectancy, so that

$$\Sigma_{ij} = [\sigma_\nu^2 + (1 - \varrho)\sigma_\tau^2 \bar{v}^2] \delta_{ij} + \varrho \sigma_\tau^2 \bar{v}^2. \quad (10)$$

The value \bar{v} is yet to be determined, so the covariances are often derived using the data in the propagation:

$$\Sigma_{ij}^* = [\sigma_\nu^2 + (1 - \varrho)\sigma_\tau^2 v_i^2] \delta_{ij} + \varrho \sigma_\tau^2 v_i v_j. \quad (11)$$

The least squares estimate for \bar{v} is given by

$$\mu^* = \frac{\mathbf{x}^T \Sigma^{*-1} \mathbf{v}}{\mathbf{x}^T \Sigma^{*-1} \mathbf{x}} \quad (12)$$

where $\mathbf{x} = (1, \dots, 1)^T$ is the trivial sensitivity vector. The covariance matrix is the sum of an invertible diagonal matrix and one of rank one—see Eq. (11)—, so that the inverse is obtained using the Woodbury matrix identity:

$$\{\Sigma^{*-1}\}_{ij} = \frac{\delta_{ij}}{\sigma_i^2} - \frac{\varrho \sigma_\tau^2 v_i v_j}{\sigma_i^2 \sigma_j^2 \left(1 + \varrho \sigma_\tau^2 \sum_k \frac{v_k^2}{\sigma_k^2}\right)}, \quad (13)$$

where

$$\sigma_i^2 = \sigma_\nu^2 + (1 - \varrho)\sigma_\tau^2 v_i^2. \quad (14)$$

It allows me to put the least squares estimate in the relatively compact form

$$\mu^* = \frac{\sum_i \frac{V_i}{\sigma_i^2}}{\sum_i \left(1 + \varrho \sigma_\tau^2 \sum_j \frac{(V_i - V_j)^2}{\sigma_j^2}\right) \frac{1}{\sigma_i^2}}. \quad (15)$$

For small enough errors ($\eta_i \ll \bar{v}$) the second-order Taylor development in $\eta_i = v_i - \bar{v}$ yields

$$\mu^* \approx \bar{v} + \frac{1}{n} \sum_i \eta_i - \frac{[2 + (n - 2)\varrho] \sigma_\tau^2 \bar{v}^2}{2n^2 \sigma^2} \sum_{i \neq j} (\eta_i - \eta_j)^2 \quad (16)$$

where

$$\bar{\sigma}^2 = \sigma_\nu^2 + (1 - \varrho)\sigma_\tau^2 \bar{v}^2 \quad (17)$$

Since $\langle \eta_i \rangle = 0$ and $\langle (\eta_i - \eta_j)^2 \rangle = 2\bar{\sigma}^2$, the expectancy

$$\langle \mu^* \rangle \approx \bar{v} \left[1 - \left(1 - \frac{1}{n}\right) (2 + (n - 2)\varrho) \sigma_\tau^2 \right] \quad (18)$$

is biased. If the data are not correlated ($\varrho = 0$), the bias is small (σ_τ^2 to $2\sigma_\tau^2$) but it becomes large for correlated data if the number of points is large ($\sim n\sigma_\tau^2$ for fully correlated data) as D’Agostini (1994) already noted. Figure 2 shows a simulation of the bias as a function of the normalisation uncertainty σ_τ for various data sizes ($n = 2$ to 100).

For spectro-interferometric observations with 4 telescopes, the number of correlated points can be over 1,000, so even with a low correlation coefficient, the impact can be large. For instance, a single GRAVITY observation in high spectral resolution yields $n = 6 \times 210$ visibility amplitudes. With an observed correlation of $\rho \approx 16\%$ in the instrumental visibility amplitudes (Kammerer et al. 2020) and a typical $\sigma_\tau = 1$ –2% normalisation error, the bias on the calibrated visibilities could be 2–8%.

4 MODEL FITTING

Let’s now consider a set of measurements corresponding to the linear model

$$\mu = \mathbf{X} \mathbf{p}, \quad (19)$$

where \mathbf{p} are the unknown parameters and \mathbf{X} is the known sensitivity matrix. Typically, $x_{ik} = f_k(u_i, v_i)$ for a linear model and $x_{ik} = \partial f / \partial p_k(u_i, v_i)$ for a non-linear model approximated by a linear one close to a solution. (u, v) is the reduced baseline. The true values $\bar{\mathbf{v}}$ are impacted by errors so that the data are

$$\mathbf{v} = \bar{\mathbf{v}} + \boldsymbol{\eta} \quad (20)$$

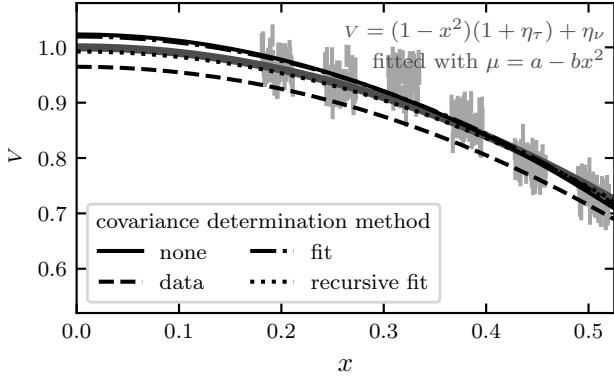
with the error term $\boldsymbol{\eta}$ again expressed as the sum of a measurement error and a normalisation one:

$$\boldsymbol{\eta} = \boldsymbol{\eta}_\nu + \boldsymbol{\eta}_\tau \odot \bar{\mathbf{v}}. \quad (21)$$

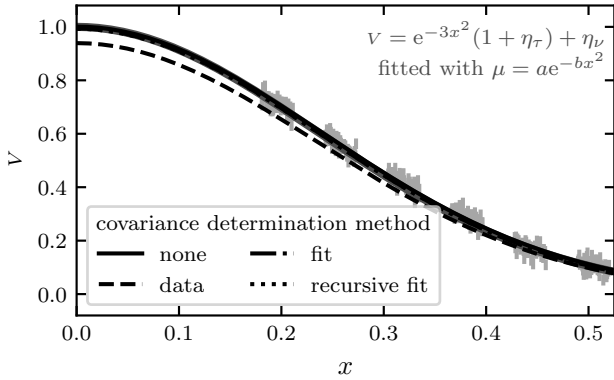
The measurement errors $\boldsymbol{\eta}_\nu$ and normalisation errors $\boldsymbol{\eta}_\tau$ following multivariate distributions of mean zero, with covariance matrices Σ_ν and Σ_τ respectively. Given the covariance matrix Σ of this model, the least squares estimate is

$$\mathbf{p} = (\mathbf{X}^T \Sigma^{-1} \mathbf{X})^{-1} (\mathbf{X}^T \Sigma^{-1} \mathbf{v}) \quad (22)$$

I investigate four ways to determine the covariance matrix



(a) Under-resolved, linear least squares



(b) Well resolved, non-linear least squares

Figure 3. Example of a fit of correlated data from a four telescope interferometer with medium resolution: 6 groups of 100 data points (light gray points with the measurement error bar) with 2% uncorrelated measurement errors and 3% correlated normalisation. *Top:* Simulated under-resolved data $v = 1 - x^2$ (thick gray line) are fitted with linear least-squares model $\mu = a - bx^2$ using the four prescriptions for the covariance matrix. *Bottom:* The same for well-resolved data $v = \exp -3x^2$ and non-linear least-squares with model $\mu = a \exp -bx^2$.

(i) Ignoring the correlations in the normalisation using $\Sigma_0 = \Sigma_\nu + (\mathbf{v} \otimes \mathbf{v}) \odot (\Sigma_\tau \odot \mathbf{I})$. Let $\mu_0 = \mathbf{X}(\mathbf{X}^T \Sigma_0^{-1} \mathbf{X})^{-1} \mathbf{X}^T \Sigma_0^{-1} \mathbf{v}$ the resulting model of the data.

(ii) Using the naïve estimate $\Sigma^* = \Sigma_\nu + (\mathbf{v} \otimes \mathbf{v}) \odot \Sigma_\tau$ which is known to lead to Peelle’s pertinent puzzle in the trivial case of a constant model.

(iii) Using the data model of the fit without the normalisation error: $\Sigma_1 = \Sigma_\nu + (\mu_0 \otimes \mu_0) \odot \Sigma_\tau$. This is the generalisation of the two-variables approach by Neudecker et al. (2014). The resulting least squares model is $\mu_1 = \mathbf{X}(\mathbf{X}^T \Sigma_1^{-1} \mathbf{X})^{-1} \mathbf{X}^T \Sigma_1^{-1} \mathbf{v}$.

(iv) Recursively fitting the data by updating the data model in the covariance matrix. I derive $\mu_k = \mathbf{X}(\mathbf{X}^T \Sigma_k^{-1} \mathbf{X})^{-1} \mathbf{X}^T \Sigma_k^{-1} \mathbf{v}$ using $\Sigma_k = \Sigma_\nu + (\mu_{k-1} \otimes \mu_{k-1}) \odot \Sigma_\tau$, starting with the estimate μ_1 ($k = 2$).

In order to compare these covariance matrix prescriptions, I will use the typical example of an under-resolved centrosymmetric source observed at a four-telescope facility in high spectral resolution. The PYTHON code to produce the re-

sults (figures in this paper) is available on github.⁷ In the under-resolved case all models—Gaussian, uniform disc, or limb-darkened disc—are equivalent (Lachaume 2003), so I will use instead a linear least squares fit $\mu = a - bx^2$ to $v \approx 1 - x^2$ where x is dimensionless variable proportional to the projected baseline length $\sqrt{u^2 + v^2}$. This fit corresponds to the second-order Taylor development of any of the aforementioned models. Figure 3(a) shows the example of such a fit performed for each covariance matrix prescription. Data have been simulated using $v = (1 - x^2)(1 + \eta_\tau) + \eta_\nu$ where η_τ is a fully correlated normalisation error (3%) and η_ν are uncorrelated statistical errors (2%). As expected, the use of data \mathbf{v} in the correlation matrix, method (ii), leads to grossly underestimated data values, in the very same way as in the classical Peelle case described in Sects. 2 & 3. Other methods, including ignoring correlations, yield reasonable fits.

Figure 4(a) sums up the behaviour of the same fit performed a large number of times on different simulated data sets, each following $v \approx 1 - x^2$. For each correlation matrix prescription, it displays the dispersion of the reduced chi squared, the model parameters a and b , and the difference between modelled value and true value. It also reports the uncertainty on model parameters given by the least squares optimisation routine in comparison to the scatter of the distribution of the values. While the model fitting ignoring correlations (i) does not show any bias, it displays a higher dispersion of model parameters and grossly underestimate the uncertainty on model parameters. The correlation matrix calculated from data (ii) is, as expected, strongly biased. Both methods estimating the correlation matrix from modelled data, (iii) & (iv), are equivalent in terms of the absence of bias, dispersion of these quantities, and correct prediction of the uncertainty on model parameters.

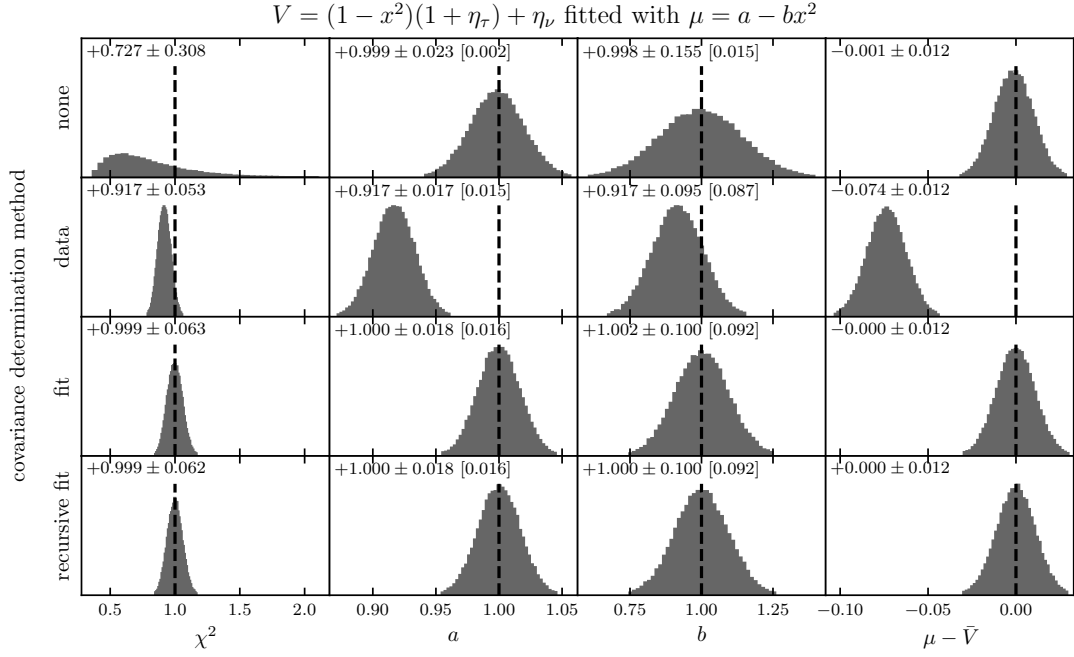
Given that fitting recursively the covariance matrix doesn’t yield additional benefits, I would suggest to use method (iii). One would expect this to hold for smooth enough non-linear least squares. Indeed, I have checked that the result holds for a fully resolved Gaussian disc $v \approx \exp -3x^2$ fit by $\mu = a \exp -bx^2$ as Figs. 3(b) & 4(b) show.

5 CONCLUSION

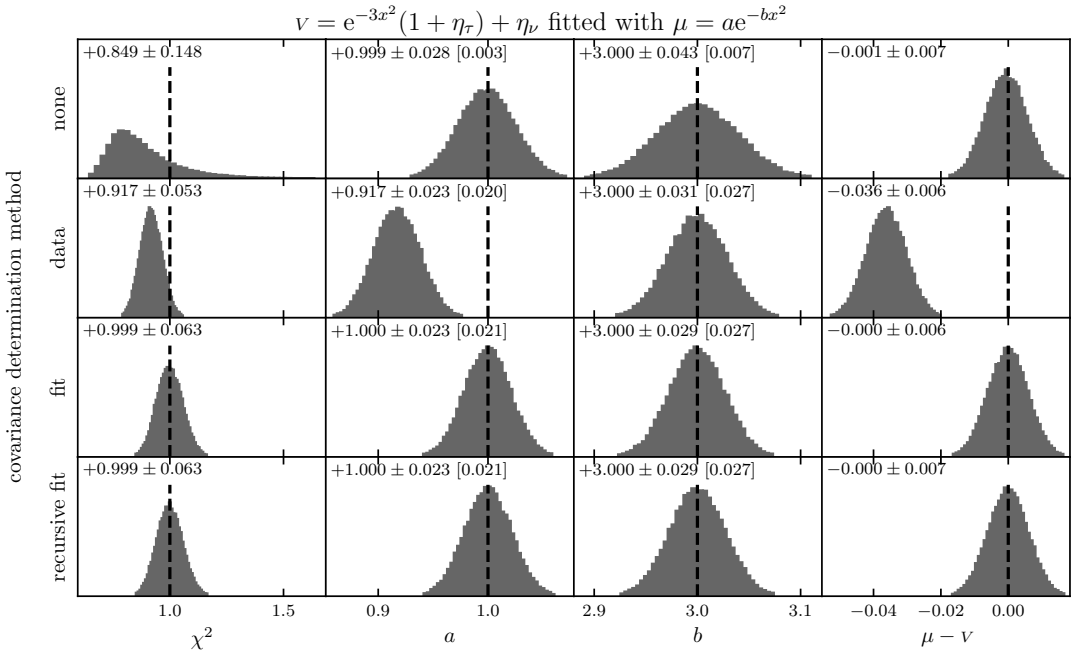
The standard, but incorrect, covariance propagation in any “normalisation” setting leads to bias in the model parameters of a least-squares fit taking correlations into account. Some bias will even occur without correlations, but the effect is strongest when a large set of correlated data is modelled. This is precisely the case in optical and infrared long-baseline interferometry, where the calibration of spectrally dispersed fringes easily yields 10^2 to 10^3 correlated data points.

While solutions exist that are either numerically expensive or require some care to be implemented (Burr et al. 2011; Becker et al. 2012; Nisius 2014), I have shown with a simple example that there is an easy and cheap way to solve the issue. First an uncorrelated fit is performed to estimate the true values corresponding to the data. Secondly, these estimates are used to determine the covariance matrix by error

⁷ <https://github.com/loqueelvientoajarez/peelles-pertinent-puzzle>



(a) Under-resolved data fitted with a linear least squares model



(b) Well-resolved data fitted with a non-linear least squares model

Figure 4. Distribution of the fitted parameters and fit properties for the four covariance matrix prescriptions. 5×10^4 simulations of 6 groups of 100 correlated data points v ($\sigma_\nu = 2\%$, $\sigma_\tau = 3\%$, $\varrho = 1$, normal distributions) are performed and fitted with a model using least-squares minimisation. *Top graph:* under-resolved data follow $v = 1 - x^2$ and are fitted with linear least squares $\mu = a - bx^2$. *Bottom graph:* well resolved data follow $v = \exp -3x^2$ and are fitted with non-linear least squares $\mu = a \exp -bx^2$. Reported quantities include median and $1\text{-}\sigma$ interval of their distribution and, within brackets, the median uncertainty reported by the least squares fit. *Leftmost column:* distribution of the least squares; *middle left:* constant coefficient a ; *middle right:* quadratic coefficient b ; *rightmost column:* mean difference between model and data. The covariance matrix prescriptions are: *top row:* correlations are ignored; *second row:* a naïve covariance matrix uses the data values; *third row:* covariance matrix uses modelled values from fit without correlations; *bottom row:* covariance matrix and model are recursively computed, with the covariance matrix of the next recursion using the modelled value of the last step.

propagation. At last, this covariance matrix is used to perform a least squares model fit.

ACKNOWLEDGEMENTS

This work has made use of the Smithsonian/NASA Astrophysics Data System (ADS) and of the Centre de Données astronomiques de Strasbourg (CDS).

REFERENCES

- Absil O., et al., 2006, *A&A*, 452, 237
- Becker B., et al., 2012, *Journal of Instrumentation*, 7, P11002
- Berger D. H., et al., 2006, *ApJ*, 644, 475
- Burr T., Kawano T., Talou P., Pan F., Hengartner N., 2011, *Algorithms*, 4, 28
- D’Agostini G., 1994, *Nuclear Instruments and Methods in Physics Research A*, 346, 306
- ESO GRAVITY pipeline team 2020, GRAVITY pipeline user manual Issue 1.4
- ESO MATISSE pipeline team 2020, MATISSE pipeline user manual Issue 1.5.1
- Eisenhauer F., et al., 2011, *The Messenger*, 143, 16
- Hummel C. A., Percheron I., 2006, in *Society of Photo-Optical Instrumentation Engineers (SPIE) Conference Series*. p. 62683X, doi:10.1117/12.671337
- Kammerer J., Mérand A., Ireland M. J., Lacour S., 2020, *A&A*, 644, A110
- Lachaume R., 2003, *A&A*, 400, 795
- Lachaume R., Rabus M., Jordán A., Brahm R., Boyajian T., von Braun K., Berger J.-P., 2019, *MNRAS*, 484, 2656
- Lawson P. R., ed. 2000, *Principles of Long Baseline Stellar Interferometry*
- Le Bouquin J.-B., et al., 2011, *A&A*, 535, A67
- Millour F., Valat B., Petrov R. G., Vannier M., 2008, in *Optical and Infrared Interferometry*. p. 701349 ([arXiv:0807.0291](https://arxiv.org/abs/0807.0291)), doi:10.1117/12.788707
- Monnier J. D., 2007, *New Astronomy Reviews*, 51, 604
- Neudecker D., Frühwirth R., Leeb H., 2012, *Nuclear Science and Engineering*, 170, 54
- Neudecker D., Frühwirth R., Kawano T., Leeb H., 2014, *Nuclear Data Sheets*, 118, 364
- Nisius R., 2014, *European Physical Journal C*, 74, 3004
- Pauls T. A., Young J. S., Cotton W. D., Monnier J. D., 2005, *PASP*, 117, 1255
- Peelle R. W., 1987, *Informal memorandum, Peelle’s Pertinent Puzzle*. Oak Ridge National Laboratory
- Perrin G., 2003, *A&A*, 400, 1173
- Perrin G., Ridgway S. T., Coudé du Foresto V., Mennesson B., Traub W. A., Lacasse M. G., 2004, *A&A*, 418, 675
- Tallon-Bosc I., et al., 2008, in *Optical and Infrared Interferometry*. p. 70131J, doi:10.1117/12.788871
- Tatulli E., et al., 2007, *A&A*, 464, 29
- Thiébaud E., 2008, in *Optical and Infrared Interferometry*. p. 70131I, doi:10.1117/12.788822